

# Hydrogenated TiO<sub>2</sub> as efficient electron transport layer of planar perovskite solar cell

Yulong Ma, Kaimo Deng, Bangkai Gu, Hao Lu, Yayun Zhu, Liang Li\*

*College of Physics, Optoelectronics and Energy, Jiangsu Key Laboratory of Thin Films, Center for Energy Conversion Materials & Physics (CECMP), Soochow University, Suzhou 215006, P. R. China*

DOI: 10.5185/amlett.2018.1944

www.vbripress.com/aml

## Abstract

The electron transport material has the great effect on the performance of hybrid perovskite solar cells. TiO<sub>2</sub> is widely chosen as the electron transport layer due to its facile synthesis and excellent charge extraction capability. Here, for the first time, we utilize the hydrogen treated TiO<sub>2</sub> as the electron transport layer for improving the performance of perovskite solar cells. The hydrogen treatment increases the Fermi level and conductivity of TiO<sub>2</sub>, and the device based on hydrogen treated TiO<sub>2</sub> exhibits a power conversion efficiency of 13.15% compared with 9.45% for the reference device with untreated TiO<sub>2</sub>. The results highlight the importance of optimizing the electron transport material and provide a new route to fabricate highly efficient planar perovskite solar cells. Copyright © 2018 VBRI Press.

**Keywords:** Electron transport layer, hydrogen treatment, TiO<sub>2</sub>, perovskite, atomic layer deposition

## Introduction

Since the first application of inorganic-organic hybrid perovskite in the field of solar cells by Miyasaka in 2009 [1], it has attracted tremendous attention due to its advantage as photovoltaic materials such as the high absorption of visible light, simple production process and large carrier mobility [2-9]. Particularly, the power conversion efficiency (PCE) of the CH<sub>3</sub>NH<sub>3</sub>PbI<sub>3</sub> (MAPbI<sub>3</sub>) perovskite solar cells (PSCs) increases from 3.8% to over 21% just within several years [1,10]. The typical PSCs include several parts: the transparent anode layer (FTO or ITO), electron transport layer (ETL), perovskite as light absorption layer, hole transport layer (HTL) and metal cathode (Au or Ag). ETL plays an important role in achieving a high PCE since it not only efficiently extracts and transports electrons from perovskite to electrode but also suppresses the recombination with holes generated in the perovskite [11,12]. TiO<sub>2</sub> thin film has been widely used as ETL in PSCs because of high light transmittance, matched energy level and thus efficient electron injection from the perovskite film to TiO<sub>2</sub> layer [13-17]. There are many methods developed to deposit TiO<sub>2</sub> thin film, such as spin coating [18], spray pyrolysis [19], sputtering [20], and atomic layer deposition (ALD) [21].

However, TiO<sub>2</sub> has a relatively low electron mobility and conductivity which may lead to a higher recombination rate and deteriorate the performance of PSCs [17]. Many efforts have been made to solve this concern. On one hand, alternative materials with a higher electron conductivity such as ZnO, SnO<sub>2</sub> and CdS have been chosen as ETL to replace the traditional TiO<sub>2</sub> layer

and comparable PCEs have been achieved [22-24]. On the other hand, modified TiO<sub>2</sub> films have also been used to improve the performance of PSCs. Snaith *et al.* adopted Al-doped TiO<sub>2</sub> as ETL to figure out this problem [25]. The conductivity of TiO<sub>2</sub> increased after Al doping, resulting in a better performance. Chen *et al.* employed Li to modify the TiO<sub>2</sub> surface, which resulted in increased conductivity of TiO<sub>2</sub> and improved PCE of devices from 14.2% to 17.1% [26]. Plenty of works indicate that modifying TiO<sub>2</sub> can obviously increase the performance of planar PSCs [27-30].

Hydrogen treatment is a simple and practical tactic that can effectively increase the conductivity and Fermi level of TiO<sub>2</sub>. The hydrogenated TiO<sub>2</sub> (H:TiO<sub>2</sub>) has been broadly applied in some fields such as water splitting, photocatalysis, photoelectrochemical sensor and lithium-ion rechargeable battery due to its excellent conductivity and optical property [31-33]. However, there are no reports about the application of hydrogen treated TiO<sub>2</sub> in perovskite solar cells. In this paper, to the best of our knowledge, we firstly employed the H:TiO<sub>2</sub> as ETL to improve the performance of PSCs. By optimizing the time and temperature of hydrogen treatment, a higher PCE of 13.15% was obtained compared to 9.45% for the reference TiO<sub>2</sub> PSCs without hydrogenation. The enhanced performance was mainly ascribed to the increased open circuit voltage and fill factor. The mechanism for the improved performance was illustrated by the systematical characterization of absorption spectra, Mott-Schottky curves, electrochemical impedance spectra and photoluminescence spectrum.

## Experimental

### Device fabrication

The FTO substrates were cleaned with detergent, acetone, ethyl alcohol and DI water in an ultrasonic bath. After the FTO substrates were treated with the O<sub>3</sub> bath for 15 min, a 10 nm thick TiO<sub>2</sub> film was deposited on the FTO substrate by ALD and annealed at 500 °C in air for 2 hours. Once cooling to room temperature, the TiO<sub>2</sub> substrates were annealed under a 5% H<sub>2</sub>/95% Ar gas flow with various temperatures of 250-500 °C for 5 hours. The TiO<sub>2</sub> substrates without hydrogenation serve as the reference devices. The perovskite films were deposited on the TiO<sub>2</sub> and H:TiO<sub>2</sub> substrates by a modified two-step vapor-assisted method. A 461 mg mL<sup>-1</sup> PbI<sub>2</sub> precursor was spin coated onto the substrate at 3000 rpm for 40 s, followed by annealing at 100 °C for 10 min. After cooling down to room temperature, the PbI<sub>2</sub> film was kept in a closed vessel containing CH<sub>3</sub>NH<sub>3</sub>I (MAI) powder for 15 min at 150 °C (the vessel was preheated for 20 min in advance). After the vapor reaction, the films were rinsed with 2-propanol afterwards and dried at 70 °C for 30 min. The spiro-OMeTAD used as the hole-transport layer was deposited on the perovskite film by spin coating at 2000 rpm for 45 s. The precursor of spiro-OMeTAD solution was prepared by adding 72.3 mg spiro-OMeTAD, 28.8 μL 4-tertbutylpyridine, and 17.5 μL lithiumbis-(trifluoromethanesulfonyl) imide (Li-TFSI) (520 mg of Li-TFSI in 1 mL acetonitrile) in 1 mL chlorobenzene. Finally, a 100 nm thick silver electrode was deposited by thermal evaporation with a shadow mask (0.12 cm<sup>2</sup> active area).

### Characterizations

The morphology of the samples was measured by a field-emission scanning electron microscope (FE-SEM) (Hitachi SU8010). The crystallization of products was checked using an X-ray diffractometer (XRD) (D/MAX-III-B-40KV, Cu K<sub>α</sub> radiation, λ = 1.5418 Å). X-ray photoelectron spectroscopy (XPS) (ESCALAB, 250Xi) was recorded for valence states.

### Property measurements

The current-voltage (*J-V*) was characterized using a Keithley source meter with a Newport solar simulator calibrated to AM1.5G (100 mW/cm<sup>2</sup>) by a standard silicon solar cell. A metal mask of 0.06 cm<sup>2</sup> was used to define the exact illumination area. External quantum efficiency (EQE) was measured with a Newport quantum efficiency system. The absorption spectra were collected by a UV-vis spectrophotometer (Shimadzu, UV-3600). The electrochemical impedance spectroscopy (EIS) was acquired with an electrochemical workstation (Autolab, PGSTAT 302N) under light at zero-bias voltages with an alternative signal amplitude of 5 mV and in the frequency range of 400 KHz to 0.01 KHz. The photoluminescence (PL) spectrum was detected with a spectrofluorometer (Horiba, Fluoromax-4) with a 525 nm excitation wavelength at room temperature.

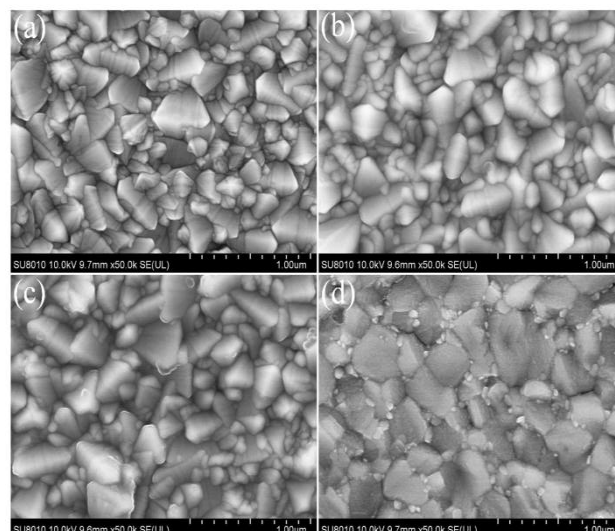


**Fig. 1.** SEM images of (a) bare FTO substrate, (b) 10 nm-thick TiO<sub>2</sub> deposited on FTO substrate by ALD, (c) Hydrogenated TiO<sub>2</sub> substrate, and (d) the perovskite film fabricated on the hydrogenated TiO<sub>2</sub> substrate.

## Result and discussion

**Fig. 1** presents the top-view scanning electron microscopy (SEM) images of bare FTO glass (**Fig. 1a**), 10 nm-thick TiO<sub>2</sub> (**Fig. 1b**), H:TiO<sub>2</sub> (**Fig. 1c**) and MAPbI<sub>3</sub> perovskite (**Fig. 1d**) films on FTO substrates. TiO<sub>2</sub> film was deposited by ALD technique and the hydrogenation reaction was conducted at 450 °C for 5 h under a mixed (5% H<sub>2</sub>/95% Ar) gas flow. The MAPbI<sub>3</sub> perovskite film was fabricated by a two-step vapor assisted synthesis method. The synthetic details can be found in the experimental section. It can be observed from the SEM images that the surface morphology of 10 nm-thick TiO<sub>2</sub> with ALD process is almost the same with the bare FTO due to the highly uniform ultrathin coating of ALD, and no obvious difference is found between the hydrogen treated and the pristine TiO<sub>2</sub>. Perovskite film is smooth and pin hole free with a large grain size.

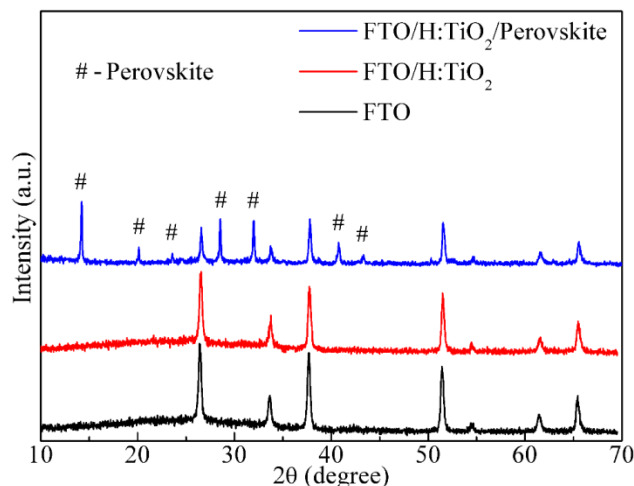


**Fig. 2** XRD patterns of FTO, FTO/H:TiO<sub>2</sub>, and FTO/H:TiO<sub>2</sub>/perovskite.

**Fig. 2** shows the corresponding X-ray diffraction (XRD) patterns for FTO, FTO/H:TiO<sub>2</sub>, and FTO/H:TiO<sub>2</sub>/MAPbI<sub>3</sub>. No distinct peaks of TiO<sub>2</sub> or H:TiO<sub>2</sub> appear because the 10 nm thickness of deposited TiO<sub>2</sub> or H:TiO<sub>2</sub> is too thin to be detected. In addition, the typical PbI<sub>2</sub> peak mainly at 12.6° is not found, indicating the complete conversion of PbI<sub>2</sub> to CH<sub>3</sub>NH<sub>3</sub>PbI<sub>3</sub>. The diffraction peaks of perovskite at 14.2°, 20.0°, 23.5°, 28.5°, 31.9°, 40.7° and 43.2° are in accordance with previous report [34]. To further confirm the existence of TiO<sub>2</sub> and change of surface bonding induced by hydrogen treatment, X-ray photoelectron spectroscopy (XPS) measurement was carried out. **Fig. 3a** shows the XPS survey spectra of O 1s core-level. The peak at 529.8 eV can be attributed to the lattice O<sup>2-</sup> in TiO<sub>2</sub>. The peak at 531.6 eV is assigned to Ti-OH which has been reported with a 1.5-1.8 eV higher binding energy than the lattice O<sup>2-</sup> core level [31]. Besides, the hydrogenated TiO<sub>2</sub> has relatively higher OH peak intensity than the TiO<sub>2</sub> without treatment, which proves the hydrogen treatment is beneficial to the formation of OH group on TiO<sub>2</sub> surface. The XPS spectra of Ti 2p core-level is shown in **Fig. 3b**. Both of the samples have an identical pattern with Ti<sup>4+</sup> peaks located at 458.6 and 464.5 eV, which is similar to other reports [31].

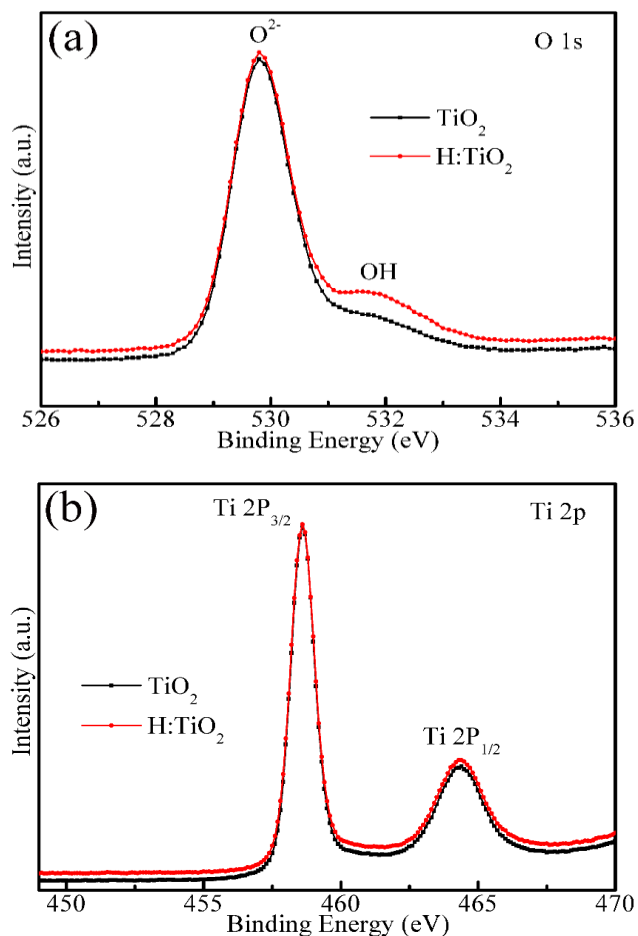


**Fig. 3.** XPS measurement of H:TiO<sub>2</sub> film. (a) and (b) are survey spectra for the O 1s and Ti 2p core-levels.

**Table 1.** Summary of photovoltaic parameters for devices with different hydrogenated temperatures and the reference TiO<sub>2</sub>.

Devices	$V_{oc}$ (V)	$J_{sc}$ (mA cm <sup>-2</sup> )	FF (%)	PCE (%)
250 °C	0.89	18.59	64.46	10.71
350 °C	0.92	19.49	64.78	11.59
450 °C	0.99	19.69	66.27	12.94
500 °C	0.85	16.78	56.51	8.09
TiO <sub>2</sub>	0.89	17.16	61.31	9.45

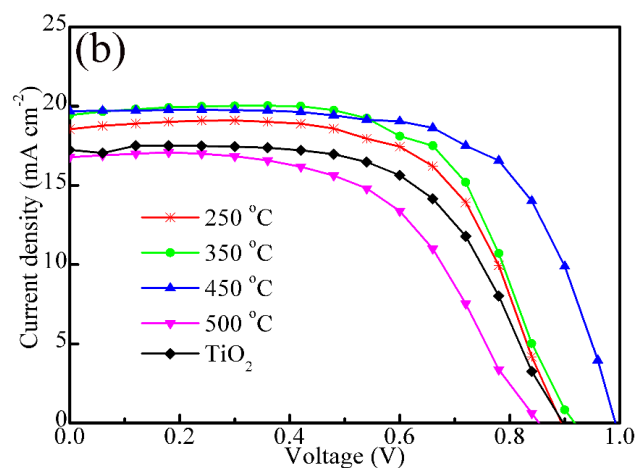
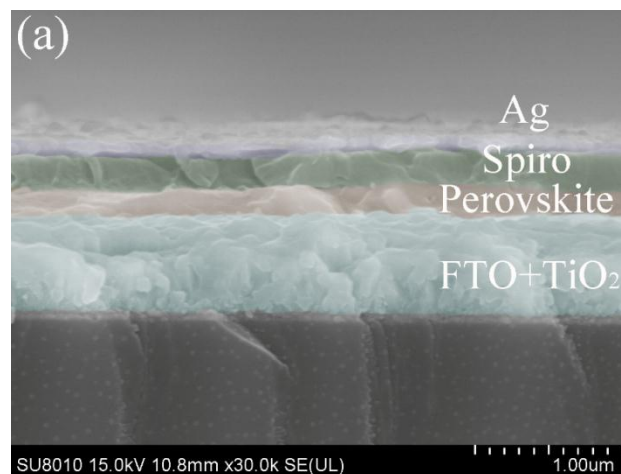


**Fig. 4.** (a) The cross-section SEM image of device. (b) *J-V* curves of the reference TiO<sub>2</sub> and H:TiO<sub>2</sub> based PSCs with different hydrogenated temperatures measured under AM 1.5G irradiation (100 mW/cm<sup>2</sup>).

The typical cross-sectional SEM image of H:TiO<sub>2</sub> based planar PSCs is shown in **Fig. 4a**, and corresponding *J-V* performance of PSCs based on H:TiO<sub>2</sub> ETLs with different hydrogen treated temperatures is shown in **Fig. 4b** together with the devices based on TiO<sub>2</sub> without hydrogenation for comparison. The corresponding photovoltaic parameters are listed in **Table 1**. The power

conversion efficiency of reference PSCs is 9.45%, with  $V_{oc}$  of 0.89 V,  $J_{sc}$  of 17.16 mA/cm<sup>2</sup> and FF of 58.93%. The performance of H:TiO<sub>2</sub> based PSCs is enhanced gradually with the hydrogenated temperature from 250 to 450 °C and then largely degraded at 500 °C. The highest performance of PSCs obtained at 450 °C has the corresponding  $V_{oc}$ ,  $J_{sc}$ , FF and PCE of 0.99 V, 19.69 mA/cm<sup>2</sup> and 66.27%, respectively. Compared with the PCE of the reference TiO<sub>2</sub> sample, all the physical parameters after hydrogen treatment are increased obviously. The definition of theoretical  $V_{oc}$  in PSCs is the difference between the Fermi level of ETL and the highest occupied molecular orbital level of HTL. The Mott-Schottky ( $M-S$ ) was used to measure the Fermi level of TiO<sub>2</sub> and H:TiO<sub>2</sub> ETLs, as shown in Fig. 5a. A positive slope in  $M-S$  plots are observed for both samples, demonstrating the feature of  $n$ -type semiconductor. More importantly, it shows that the Fermi level of TiO<sub>2</sub> drops from -0.633 to -0.826 V by fitting the curves, suggesting that the Fermi level of ETLs is increased after hydrogen treatment. This phenomenon agrees well with the increase in  $V_{oc}$  for the PSCs. Moreover, the H:TiO<sub>2</sub> sample shows a smaller slope of  $M-S$  plot compared to the reference TiO<sub>2</sub>, which means the donor densities of TiO<sub>2</sub> after hydrogen treatment are increased. According to the equation [35]

$$N_D = \left(\frac{2}{\varepsilon\varepsilon_0 e}\right) [d(1/C^2)/d(V)]^{-1}$$

where  $N_D$  is the donor density,  $\varepsilon$  is the dielectric constant of TiO<sub>2</sub>,  $\varepsilon_0$  is the permittivity of vacuum,  $e$  is the electron charge,  $C$  is the capacitance of the space charge region and  $V$  is the applied voltage at the electrode, the donor density of TiO<sub>2</sub> and H:TiO<sub>2</sub> samples are calculated to be  $4.09 \times 10^{20}$  and  $7.82 \times 10^{20}$  cm<sup>-3</sup>, respectively. Obviously, the donor density is increased due to the increased OH groups after hydrogen treatment, and thus the electrical conductivity of TiO<sub>2</sub> is improved. To further confirm the increased oxygen vacancies, the  $J-V$  curves of TiO<sub>2</sub> and H:TiO<sub>2</sub> films were measured in hole-only devices under the dark condition (Fig. 5b). Clearly, the current increases linearly with voltage at the lower bias voltage, which indicates the ohmic response of devices. At the higher bias voltage, the current increases nonlinearly, suggesting that the trap states are fully filled. The trap filled limit transition points ( $V_{TFL}$ ) linearly vary with the trap-state density and is determined by the equation [36]

$$V_{TFL} = \frac{en_t L^2}{2\varepsilon\varepsilon_0}$$

where  $e$  is the electron charge,  $n_t$  is the trap-state density,  $L$  is the thickness of TiO<sub>2</sub> film,  $\varepsilon$  is the dielectric constant of TiO<sub>2</sub> and  $\varepsilon_0$  is the permittivity of vacuum. The  $V_{TFL}$  value of H:TiO<sub>2</sub> is 0.84 V, larger than that of 0.48 V of TiO<sub>2</sub>, indicating that the trap density increases after

hydrogenation, considering the other parameters are the same. In other words, the oxygen vacancies increase after hydrogen treatment, which agrees well with XPS results above. To further confirm the increased conductivity of samples after hydrogenation, the resistance of TiO<sub>2</sub> and H:TiO<sub>2</sub> based substrates were measured. The resistance of H:TiO<sub>2</sub> is 5.2 Ω, significantly lower than 26 Ω for the pristine TiO<sub>2</sub>.

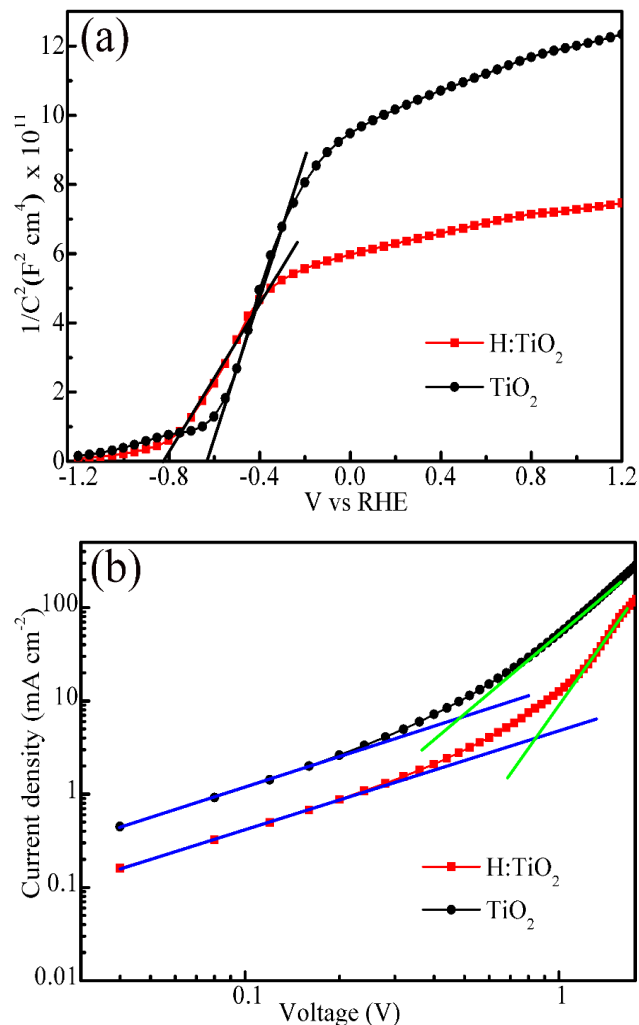
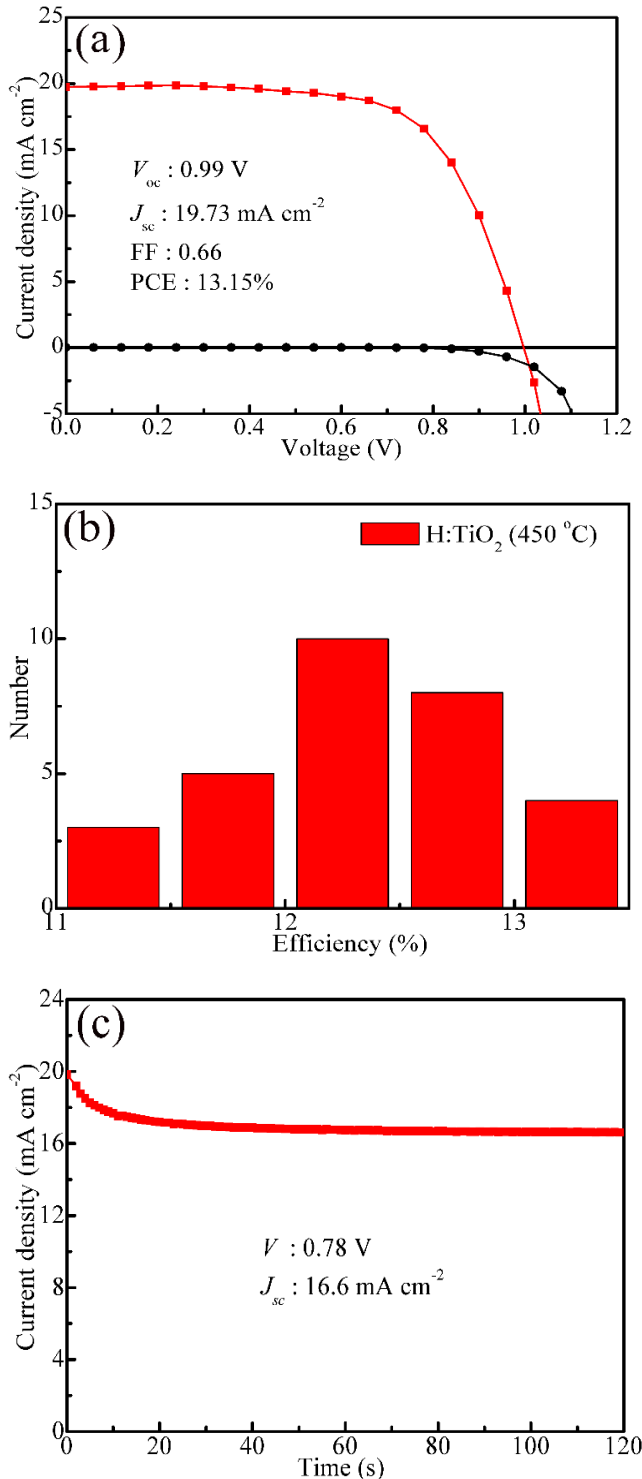


Fig. 5 (a)  $M-S$  curves of TiO<sub>2</sub> and H:TiO<sub>2</sub> electrodes. (b) Dark  $J-V$  curves of the hole-only devices.

When the hydrogenated temperature exceeds 450 °C, the performance of devices decreases dramatically, which is primarily attributed to the increased resistance of FTO substrate as the hydrogenated temperature is higher than 450 °C. The corresponding resistance of the FTO substrate after hydrogen treatment at 500 °C is 398 Ω, which is much higher than the pristine FTO. The same phenomenon was also observed in the previous report [31]. Therefore, 450 °C is served as the optimal hydrogenated temperature in our work. The PCEs from 30 devices with the optimum hydrogenated temperature were obtained to evaluate the reproducibility of PSCs. As

shown in **Figs 6a and 6b**, the champion device has a PCE of 13.15% and the average value is 12.32%. The output current density at the maximum power point of the champion device is shown in **Fig. 6c**. The corresponding stable PCE is 12.95%, which is consistent with the PCE from the *J-V* curve.



**Fig. 6.** (a) *J-V* curve of the H:TiO<sub>2</sub> (450 °C) based PSC with the highest efficiency under AM 1.5G illumination and in the dark. (b) Histogram of PCEs measured from 20 H:TiO<sub>2</sub> based devices. (c) The output current density at the maximum power point of the champion device (0.78 V).

The ultraviolet-visible (UV-vis) absorption spectra of FTO/TiO<sub>2</sub>/MAPbI<sub>3</sub> and FTO/H:TiO<sub>2</sub>/MAPbI<sub>3</sub> were carried out to explore whether the optical properties of devices were changed after the hydrogen treatment. In **Fig. 7a**, the intensity of the absorption curves is almost the same in the whole wavelength range for two samples. In contrast, the external quantum efficiency (EQE) curves (**Fig. 7b**) of PSCs show a significant difference with the integrated *J<sub>sc</sub>* to be 15.80 and 18.14 mA/cm<sup>2</sup>, respectively. It is well known that the EQE as well as the *J<sub>sc</sub>* values are intimately related to the light harvesting and charge collection efficiencies. Since there is little influence on the light absorption after the TiO<sub>2</sub> hydrogenation, the dynamics of charge transport may be responsible for the different EQE.

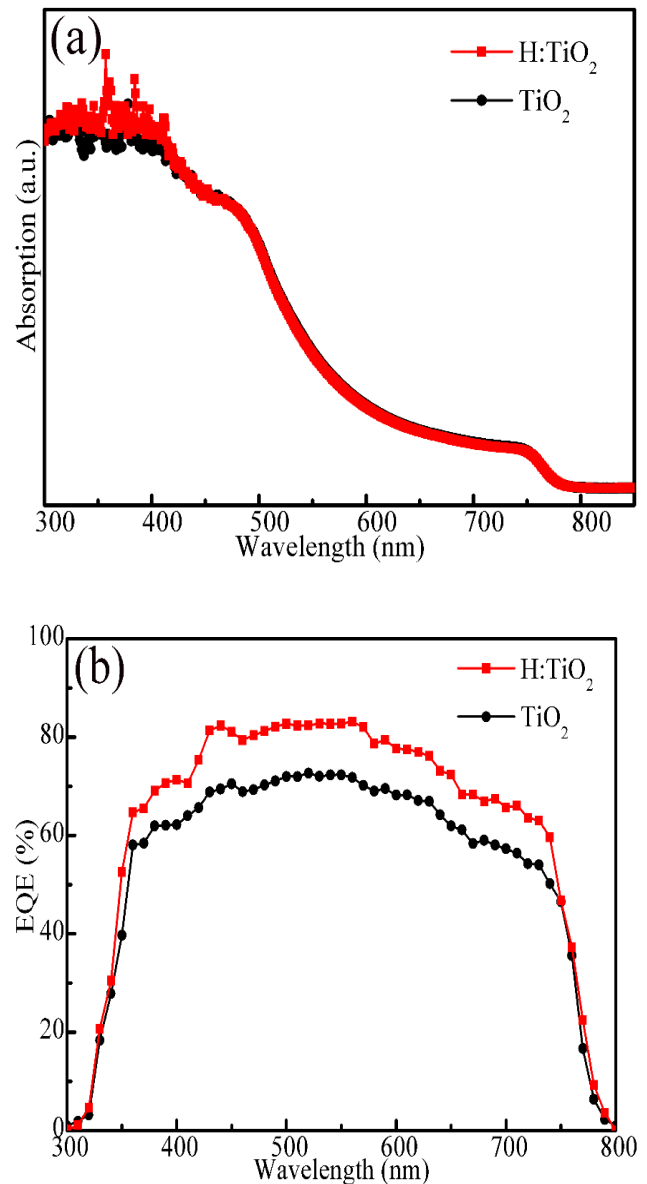


**Fig. 7.** (a) UV-vis absorption spectra of perovskite films coated on TiO<sub>2</sub> and H:TiO<sub>2</sub> substrates. (b) EQE measurement of H:TiO<sub>2</sub> with 450 °C hydrogenated temperature based PSC and the reference TiO<sub>2</sub> device.

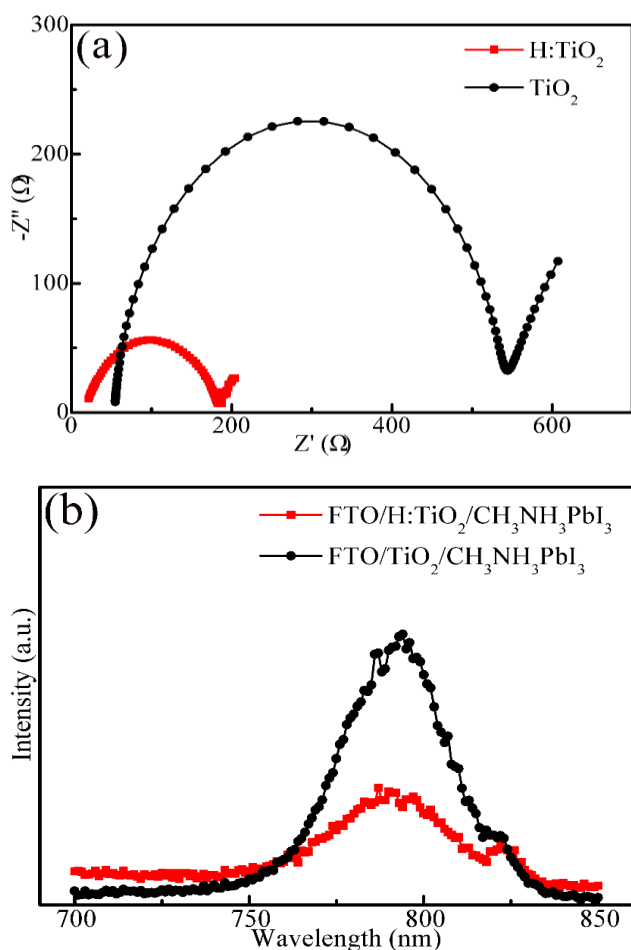


**Fig. 8.** Nyquist plots of (a) H:TiO<sub>2</sub> and reference TiO<sub>2</sub> based PSCs measured under AM 1.5G illumination. (b) PL spectra of the pristine perovskite films deposited on TiO<sub>2</sub> and H:TiO<sub>2</sub> coated FTO substrates.

Electron impedance spectroscopy (EIS) was measured to uncover the charge transport and recombination process in PSCs. **Fig. 8a** shows the Nyquist plots of TiO<sub>2</sub> and H:TiO<sub>2</sub> (450 °C) based PSCs under AM 1.5G illumination, and the corresponding equivalent circuit model is inserted in the top-right corner. Two main arcs are observed clearly from the Nyquist plots with one at the high-frequency range and the other at the lower-frequency range. Three components constitute the equivalent circuit: the series resistances ( $R_s$ ),  $Z_1$  consisted of  $R_1$  and the relevant capacitors (CPE1), and  $Z_2$  including  $R_{rec}$  and capacitor (CPE2). The  $R_1$  at the high-frequency region stands for the transport resistance at the ETL/perovskite or HTL/perovskite interface. In our work, the  $R_1$  represents the transport resistance at the ETL/perovskite interface since both the architecture of PSCs have the same perovskite/HTL interface. The  $R_{rec}$  at the lower-frequency region represents the recombination resistance. The values of resistances extracted from Nyquist plots are summarized in **Table 2**. It is shown that the series resistances of devices decrease from 54 to 16 Ω after hydrogenation compared with the untreated TiO<sub>2</sub> based PSCs. The series resistance directly affects the FF

of PSCs, and a lower series resistance favors a larger FF which is consistent with the above *J-V* test. The  $R_1$  of H:TiO<sub>2</sub> based device decreases from 484 to 170 Ω compared with the untreated sample, demonstrating that the electron transport and extraction become more efficient at the ETL/perovskite interface after hydrogenation. To further confirm this result, steady-state photoluminescence (PL) was performed to investigate the electron transport process at the ETL/perovskite interface. **Fig. 8b** shows the PL of FTO/TiO<sub>2</sub>/MAPbI<sub>3</sub> and FTO/H:TiO<sub>2</sub>/MAPbI<sub>3</sub>. The emission peak for both samples is observed at around 790 nm consistent with the previous study. The peak quenching effect for H:TiO<sub>2</sub> based device is more serious than the reference TiO<sub>2</sub>, implying more effective electron transfer at the H:TiO<sub>2</sub>/perovskite interface. The  $R_{rec}$  is inversely proportional to the recombination rate in PSCs. It is worthy to note that the values of  $R_{rec}$  increase distinctly from 731 to 2140 Ω. Therefore, the recombination rates are reduced by hydrogenating the TiO<sub>2</sub>. Furthermore, the EIS of PSCs based on TiO<sub>2</sub> hydrogenated at different temperatures was studied under the light illumination (**Fig. S1**) and the corresponding values of  $R_s$ ,  $R_1$  and  $R_{rec}$  are listed in **Table S1**. Increasing the hydrogenated temperature, the values of  $R_s$  and  $R_1$  decrease and  $R_{rec}$  increase gradually, because the higher temperature makes the hydrogenation more efficient, except for the H:TiO<sub>2</sub> (500 °C) based devices because of the damaged FTO substrates at this temperature. Based on the above analysis, we propose that the facile hydrogen treatment of TiO<sub>2</sub> ETLs is an efficient route to obtain a more efficient charge transport and a lower recombination rate in planar perovskite solar cells.

**Table 2.** Summary of EIS parameters of H:TiO<sub>2</sub> (450 °C) and reference TiO<sub>2</sub> devices.

Devices	$R_s$ (Ω)	$R_1$ (Ω)	$R_{rec}$ (Ω)
H:TiO <sub>2</sub>	16.1	170	2140
TiO <sub>2</sub>	54	484	731

## Conclusions

In summary, we have demonstrated a new hydrogenation method to treat the TiO<sub>2</sub> ETLs for enhancing the performance of planar PSCs. A champion PCE of 13.15% is achieved at the optimum hydrogenated temperature (450 °C) compared with 9.45% for the reference TiO<sub>2</sub> based device. The enhanced performance after hydrogenation is attributed to more efficient charge extraction and lower recombination rates existed at the ETL/perovskite interface, which is related to the raised Fermi level and conductivity of TiO<sub>2</sub>. Our results open a new and promising method to engineer the ETL/perovskite interface and improved performance can be manipulated from the point of interface energy band engineering.

**Acknowledgments**

This research was supported by the National Natural Science Foundation of China (51772197, 51422206, 51372159), 1000 Youth Talents Plan, Key University Science Research Project of Jiangsu Province (17KJA430013), 333 High-level Talents Cultivation Project of Jiangsu Province, Six Talents Peak Project of Jiangsu Province, Distinguished Young Scholars Foundation by Jiangsu Science and Technology Committee (BK20140009), and Funded by the Priority Academic Program Development of Jiangsu Higher Education Institutions (PAPD).

**Reference**

1. Kojima, A.; Teshima, K.; Shirai, Y.; Miyasaka, T.; *J. Am. Chem. Soc.* **2009**, 131, 6050.
2. Lee, M. M.; Teuscher, J.; Miyasaka, T.; Murakami, T. N.; Snaith, H. J.; *Science* **2012**, 338, 643.
3. Burschka, J.; Pellet, N.; Moon, S.; Humphry-Baker, R.; Gao, P.; Nazeeruddin, M. K.; Grätzel, M.; *Nature* **2013**, 499, 316.
4. Zhou, H.; Chen, Q.; Li, G.; Luo, S.; Song, T.; Duan, H.; Hong, Z.; You, J.; Liu, Y.; Yang, Y.; *Science* **2014**, 345, 542.
5. Lee, J. W.; Seol, D. J.; Cho, A. N.; Park, N. G.; *Adv. Mater.* **2014**, 26, 4991.
6. Hao, F.; Stoumpos, C. C.; Cao, D. H.; Chang, R.; Kanatzidis, M. G.; *Nature Photon.* **2014**, 8, 489.
7. Heo, J. H.; Song, D. H.; Im, S. H.; *Adv. Mater.* **2014**, 26, 8179.
8. Dong, Q.; Fang, Y.; Shao, Y.; Mulligan, P.; Qiu, J.; Cao, L.; Huang, J.; *Science* **2015**, 347, 967.
9. Kim, H. D.; Ohkita, H.; Benten, H.; Ito, S.; *Adv. Mater.* **2015**, 28, 917.
10. Bi, D. Q.; Yi, C. Y.; Luo, J. S.; Decoppet, J.-D.; Zhang, F.; Zakeeruddin, S. M.; Li, X.; Hagfeldt, A.; Grätzel, M.; *Nature Energy* **2016**, 1, 16142.
11. Stranks, S.D.; Snaith, H. J.; *Nature Nanotech.* **2015**, 10, 391.
12. Snaith, H. J.; *J. Phys. Chem. Lett.* **2013**, 4, 3623.
13. Saliba, M.; Matsui, T.; Seo, J.-Y.; Domanski, K.; Correa-Baena, J.-P.; Nazeeruddin, M. K.; Zakeeruddin, S. M.; Tress, W.; Abate, A.; Hagfeldt, A.; Grätzel, M.; *Energy Environ. Sci.* **2016**, 9, 1989.
14. Yang, W. S.; Noh, J. H.; Jeon, N. J.; Kim, Y. C.; Ryu, S.; Seo, J.; Seok, S.I.; *Science* **2015**, 348, 1234.
15. Ahn, N.; Son, D. Y.; Jang, I. H.; Kang, S. M.; Choi, M.; Park, N. G.; *J. Am. Chem. Soc.* **2015**, 137, 8696.
16. Heo, J. H.; Han, H. J.; Kim, D.; Ahn, T. K.; Im, S. H.; *Energy Environ. Sci.* **2015**, 8, 1602.
17. Yang, G.; Tao, H.; Qin, P.; Ke, W.; Fang, G.; *J. Mater. Chem. A* **2016**, 4, 3970.
18. Seo, M.-S.; Jeong, I.; Park, J.-S.; Lee, J.; Han, I. K.; Lee, W. I.; Son, H. J.; Sohn, B.-H.; Ko, M. J.; *Nanoscale* **2016**, 8, 11472.
19. Heo, J. H.; Lee, M. H.; Han, H. J.; Patil, B. R.; Yu, J. S.; Im, S. H.; *J. Mater. Chem. A* **2016**, 4, 1572.
20. Yang, D.; Yang, R.; Zhang, J.; Yang, Z.; Liu, S.; Li, C. *Energy Environ. Sci.* **2015**, 8, 3208.
21. Lu, H.; Ma, Y.; Gu, B.; Tian, W.; Li, L.; *J. Mater. Chem. A* **2015**, 3, 16445.
22. Chandiran, A. K.; Abdi-Jalebi, M.; Yella, A.; Dar, M. I.; Yi, C. Y.; Shivashankar, S. A.; Nazeeruddin, M. K.; Grätzel, M.; *Nano Lett.* **2014**, 14, 1190.
23. Ke, W. J.; Fang, G. J.; Liu, Q.; Xiong, L. B.; Qin, P. L.; Tao, H.; Wang, J.; Lei, H. W.; Li, B. R.; Wan, J. W.; Yang, G.; Yan, Y. F.; *J. Am. Chem. Soc.* **2015**, 137, 6730.
24. Liu, J.; Gao, C.; Luo, L.; Ye, Q.; He, X.; Ouyang, L.; Guo, X.; Zhuang, D.; Liao, C.; Meia, J.; Lau, W.; *J. Mater. Chem. A* **2015**, 3, 11750.
25. Pathak, S. K.; Abate, A.; Ruckdeschel, P.; Roose, B.; Godel, K. C.; Vaynzof, Y.; Santhala, A.; Watanabe, S.-I.; Hollman, D. J.; Noel, N.; Sepe, A.; Wiesner, U.; Friend, R.; Snaith, H. J.; Steiner, U.; *Adv. Funct. Mater.* **2014**, 24, 6046.
26. Liu, D.; Li, S.; Zhang, P.; Wang, Y.; Zhang, R.; Sarvari, H.; Wang, F.; Wu, J.; Wang, Z.; Chen, Z. D.; *Nano Energy* **2017**, 31, 462.
27. Wu, M. C.; Chan, S. H.; Jao, M. H.; Su, W. F.; *Sol. Energy Mater. Sol. Cells* **2016**, 157, 447.
28. Li, Y.; Cooper, J. K.; Liu, W.; Sutter-Fella, C.M.; Amani, M.; Beeman, J. W.; Javey, A.; Ager, J. W.; Liu, Y.; Toma, F.M.; Sharp, I. D.; *Nat. Commun.* **2016**, 7, 12446.
29. Yin, X.; Guo, Y.; Xue, Z.; Xu, P.; He, M.; Liu, B.; *Nano Res.* **2015**, 8, 1997.
30. Nagaoka, H.; Ma, F.; deQuilettes, D. W.; Vorpahl, S. M.; Glaz, M. S.; Colbert, A. E.; Ziffer, M. E.; Ginger, D. S.; *J. Phys. Chem. Lett.* **2015**, 6, 669.
31. Wang, G.; Wang, H.; Ling, Y.; Tang, Y.; Yang, X.; Fitzmorris, R.; Wang, C.; Zhang, J.; Li, Y.; *Nano Lett.* **2011**, 11, 3026.
32. Heller, A.; Degani, Y.; Johnson, D. W.; Gallagher, P. K.; *J. Phys. Chem.* **1987**, 91, 5987.
33. Shin, J.-Y.; Joo, J. H.; Samuelis, D.; Maier, J.; *Chem. Mater.* **2012**, 24, 543.
34. Ma, Y.; Deng, K.; Gu, B.; Cao, F.; Lu, H.; Zhang, Y.; Li, L.; *Adv. Mater. Interfaces* **2016**, 3, 1600729.
35. Tamirat, A. G.; Su, W.-N.; Dubale, A. A.; Chen, H.-M.; Hwang, B. J.; *J. Mater. Chem. A* **2015**, 3, 5949.
36. Yang, D.; Yang, R.; Ren, X.; Zhu, X.; Yang, Z.; Li, C.; Liu, S.; *Adv. Mater.* **2016**, 28, 5206.